Supporting Information for:

Graphene setting the stage: Following DNA hybridization with Nanoscale Resolution

Ricardo M. R. Adão[1], Rui Campos[2, ‡] , Edite Figueiras[1, $] , Pedro Alpuim[2,3] and Jana B. Nieder[1,2]

[1] Department of Nanophotonics, Ultrafast Bio- and Nanophotonics Group, INL - International Iberian Nano-technology Laboratory, Av. Mestre José Veiga s/n, 4715-330, Braga, Portugal
[2] Department of Quantum & Energy Materials, 2D Materials and Devices Group, INL - International Iberian Nanotechnology Laboratory, Av. Mestre José Veiga s/n, 4715-330, Braga, Portugal
[3] Department of Physics, University of Minho, Campus de Gualtar, 4710-057, Braga, Portugal
E-mail: jana.nieder@inl.int

Received xxxxxx
Accepted for publication xxxxxx
Published xxxxxx

Keywords: Biosensor, Optical Biosensor, Nanoruler, FLIM, Fluorescence quenching, Axial super-resolution

S1. Complementary morphological and Raman characterization of graphene samples

Large-area dark-field optical microscopy images (Eclipse LV100ND, Nikon) of the CVD-Grown graphene enabled tracing the surface coverage of the graphene, revealing the formation of flakes (figure S1(a)) which are of particular interest for the study of the spatial distribution of the DNA binding on the graphene surface. Confocal Raman spectroscopy mappings were taken (Alpha 300R, Witec) inside graphene flakes (figure S1(b)) revealed homogeneous surface coverage of monolayer graphene with relatively small number of defects ($I_{2D}/I_G = 2$, figure S1(c)).

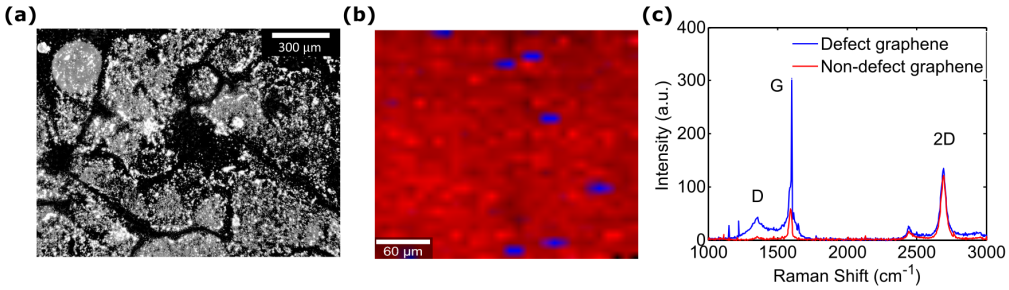

Figure S1. Optical Characterization of graphene. (a) Dark-field optical microscopy image of graphene sheet showing the formation of flakes. (b) Confocal Raman spectroscopy mapping of spectral correlation with the red and blue spectra plotted in (c), within a single graphene flake. Low intensity of D peak and ratio I_{2D}/I_G =2 for the spectrum plotted in red indicates non-defective monolayer graphene. Red and blue areas in (b) thereby reveal the presence of non-defective and defective areas, respectively.

S2. Estimation of DNA strand length in unfolded configuration

The sequence used for the DNA probe is shown in figure S2, along with the reaction with the PBSE ester, which connects the hp molecular beacon to the graphene. The bond length between each pair of atoms can be used to approximate the length of the PBSE linker by[1]

$$z_{\text{linker}} \approx 3z_{\text{C-C}} + 2z_{\text{C-N}} + 6z_{\text{C-C}} = 1.7 \text{ nm} \quad (1)$$

and that of probe DNA [2] by

$$z_{\text{DNA}} \approx 29z_{(\text{adjacent nucleobases})} \approx 10.5 \text{ nm} \quad (2)$$

During an unfolding reaction we expect the DNA-attached Atto-488 label to change its relative distance to graphene by 10.5 nm, The minimum initial distance is expected to be 1.7 nm which only considers the PBSE linker but does not account for any physical extension of the Atto488 dye and the link of the dye to the DNA itself.

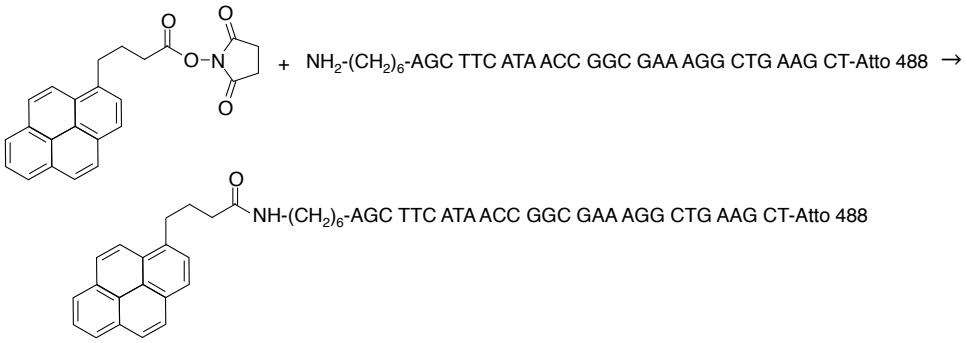

Figure S2. Schematic of conjugation of NHS-Ester modification to amino-labeled oligonucleotide with DNA sequence corresponding to the fluorophore-labeled (Atto488) molecule used in the biosensing experiments

S3. Distance-dependence of the fluorescence lifetime in the near field of graphene: theoretical model

A. Conversion from fluorescence lifetime values into nanometer distances from graphene

Fluorophores in solution have a free-space decay rate Γ_0 given by the sum of intrinsic radiative and non-radiative decay rates: $\Gamma_0 = \Gamma_r + \Gamma_{nr}$. When the fluorophore is located at the near-field distance from an energy acceptor such as graphene, non-radiative energy transfer from the fluorophore to the acceptor can occur, which modifies its decay rate of the fluorophore to:

$$\Gamma = \Gamma_0 + \Gamma_q \quad (3)$$

with Γ_q the quenching rate proportional to the energy transfer.

This effect is known by Resonant Energy Transfer (RET), first proposed and theoretically described by Theodor Förster, for a dipole-dipole intermolecular energy transfer.[3]

The electromagnetic coupling between acceptor and donor depends on the alignment of their electronic dipole moments. Therefore, the distance-dependence of the energy transfer efficiency, and thus of the quenching rate, dramatically changes with donor and acceptor geometry factors and dimensionality[4,5]

$$\Gamma_q = \Gamma_0 \left(\frac{R_0}{z}\right)^{n+3} \quad (4)$$

Here n is the dimensionality coefficient, R_0 is the Förster radius and z is the distance between donor and acceptor. In this sense, n is the number of constrained dimensions (n = 1 for 2D graphene surface) and R_0 is the distance at which the probability of an excited molecule to decay to its ground state by fluorescence or any non-radiative process is equal to the probability of transferring its energy to an acceptor.[6] Therefore, R_0 is the distance at which Γ_q becomes equal to Γ_0. Gaudreau et al. theoretically formulated the Förster radius R_0 for the interaction between a point-dipole and graphene (which can be visualized as a two-dimensional hexagonal lattice of point-dipole acceptor oscillators), with a power-of-four dependence with distance z,[7,8] expressed in the form of:[9]

$$\frac{\Gamma(z)}{\Gamma_0} = 1 + \frac{9\nu\alpha}{256\pi^3(\epsilon+1)^2}\left(\frac{\lambda}{z}\right)^4 \quad (5)$$

where ν is the relative dipole orientation factor, α is the fine structure constant (α = 1/137), ε is the dielectric constant of the medium and λ is the emission wavelength of the fluorophore. Equivalently, the dependence of the fluorescence lifetime τ with distance can be expressed using the relation ($\tau = 1/\Gamma$), where Equation (5) becomes

$$\tau(z)/\tau_0 = 1/\left(1 + \frac{9\nu\alpha}{256\pi^3(\epsilon+1)^2}\left(\frac{\lambda}{z}\right)^4\right) \quad (6)$$

In this article, we use the inverse function of Equation 6 to calculate the distance between Atto 488 fluorophores and a graphene surface by converting experimentally measured fluorescence lifetime values into nanoscale distance information:

$$z(\tau) = \lambda \left[\frac{9\nu\alpha}{256\pi^3(\epsilon+1)^2} / \left(\frac{\tau_0}{\tau} - 1 \right) \right]^{1/4} \qquad (7)$$

where $\alpha \approx 1/137$;[10,11] the fine structure constant , $\nu = 1.5$, the orientation coefficient considering isotropic emission of the dye,[9] $\varepsilon = 2.19$ for SiO2[12] (verification sample) and $\varepsilon = 1.88$ for the trisodium citrate buffer solution[13](biofunctionalized sample) the effective dielectric constant, calculated by folding the material dielectric function against the emission spectrum of Atto-488[14] and $\lambda = 542.7$ nm its average emission wavelength. The free space fluorescence lifetime of $\tau_0 = 4.3$ ns was determined experimentally using Atto 488-doped PVA thin film on glass.

S4. FLIM images taken at each spacer thickness of the nanofabricated verification sample

In figure S3 we show the FLIM images associated to the data shown in figure 2 of the main text. The excellent agreement between the experimentally determined lifetimes measured at z < 10 nm and the theoretical model (Equation 6) is highlighted in the Log-Log plot of figure S4.

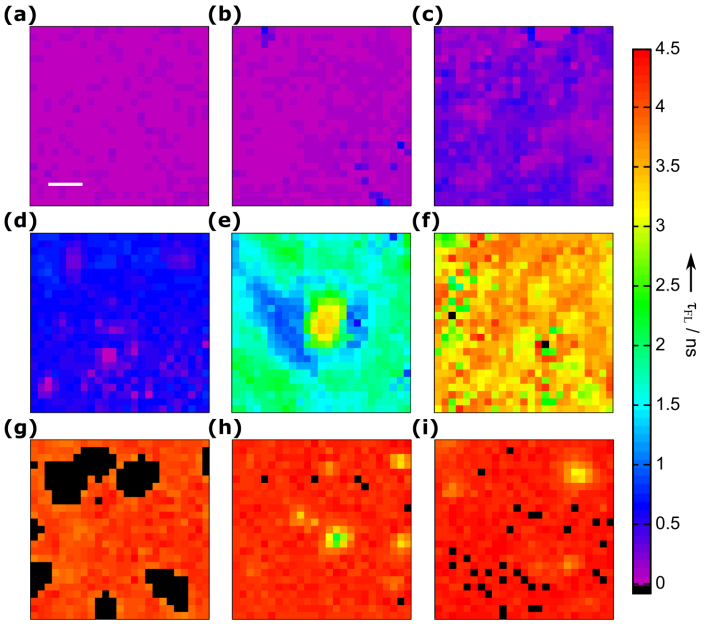

Figure S3. FLIM images taken for Atto488 in PVA separated by different SiO_2 spacer thicknesses from the graphene. (a) 0 nm (directly on graphene), (b) 4 nm, (c) 8 nm, (d) 12 nm, (e) 16 nm, (f) 24 nm, (g) 32 nm, (h) 40 nm, i) 48 nm. The scale bar is 10 µm. Pixels in black are indicating areas that were excluded from the FLIM analysis, because of intensity characteristics, indicating presence of impurities or other deviations from a homogenous dye layer in these areas.

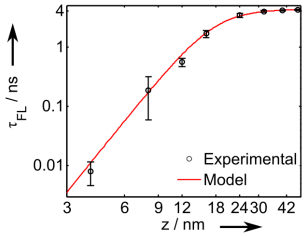

Figure S4. Log-log scale comparison between the experimental fluorescence lifetime as function of nanoscale distance to graphene, with a theoretical z^{-4} distance-dependence RET model developed for graphene by Gaudreau et al.[17]

S5. Analysis of film roughness using nanoscale sensitivity

To evaluate the roughness of the PECVD-grown SiO_2, excluding any other contributions (such as graphene wrinkles, glass roughness, PVA furrows etc.) we deposited SiO_2 steps of 15, 30, 45 and 60 nm on Si wafer substrate (roughness R_{RMS} = 0.18 ± 0.03 nm) and acquired the AFM images shown in Figure S5 (a-e). We verify that the roughness increases exponentially with the thickness (see Figure S5 (f)), as previously reported [15] . We also observe a roughness of 0.36 ± 0.06 @ t = 30 nm, which indicates that the SiO_2 roughness is small.

The AFM images of the experimental verification sample (glass + graphene + SiO_2 + PVA Atto488) at each of the spacer layers are shown in Figure S6 (a-h). Additionally we provide a plot of the roughness in dependence of the spacer thickness in Figure S6 (i). For the multilayer verification sample generally a larger roughness is observed starting with R_{RMS} = 1.8 ± 0.8 nm @ t = 0 nm, where the PVA Atto488 layer is deposited directly on top of graphene on a cover glass substrate.

The roughness reaches up to 7 ± 2 nm @ t=40 nm, which compared to the roughness found for Si + SiO2 sample at a similar thickness of t=45 nm has a R_{RMS} =0.7 ± 0.2 (dashed blue line) is large, however, it is still well below the nominal thickness for all spacer layers (black line, R_{RMS} = t).

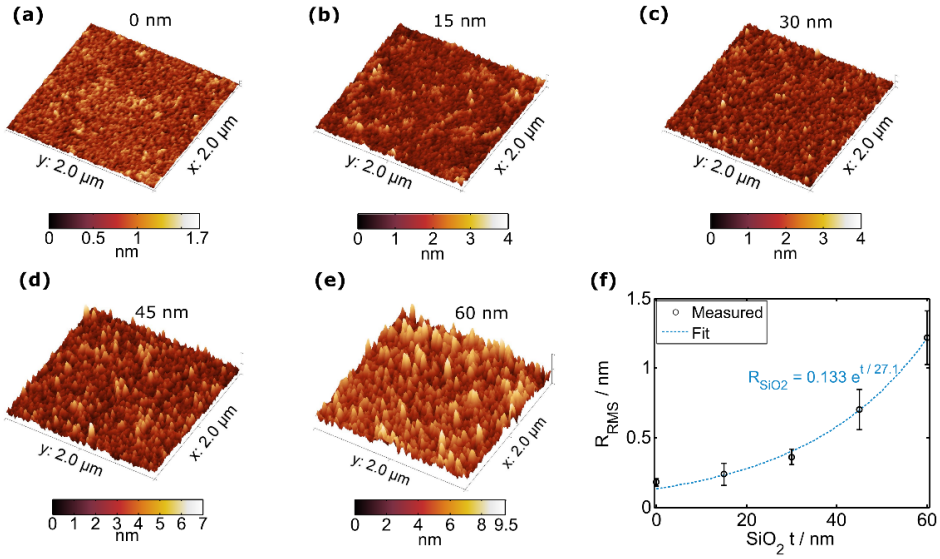

Figure S5. AFM images of SiO_2 on top of Si substrate. (a) Directly on Si. (b-e) SiO2 thickness of 15, 30, 45 and 60 nm. (f) Plot of RMS roughness as function of the SiO_2 thickness and exponential curve fitting.

The roughness should have a direct impact on the width of the fluorescence lifetime distribution associated to a FLIM image collected in each spacer layer. To assess the effect of sample roughness on our fluorescence lifetime measurements, we compare the widths (standard deviations) of the fluorescence lifetime distributions (shown in Figure 2c of the main text) obtained for the difference spacer thicknesses. One can distinguish 3 different regimes: i) extremely narrow distributions of $\sigma < 0.13$ ns at short distances (0 - 12 nm nominal distances); ii) broader lifetime distributions of σ from 0.15 to 0.24 ns for intermediate distances of nominal 16, 24, 32 nm and iii) narrow distributions σ around 0.1 ns for distances of nominal (40 and 48 nm).

In figure S7 (a) we plot the width of the fluorescence lifetime distributions in dependence of the nominal spacer layer thickness. In the narrow width regime i) all Atto 488 molecules are in a strong quenching distance from the Graphene, where indeed some are completely quenched (as expected for distances between 0 and 6 nm from Graphene (see theoretical model in figure 2 (d) in the main text). We can use the measured variance of the fluorescence lifetimes per FLIM image to estimate the range of distances of Atto 488 molecules from the quenching Graphene sheet, within each spacer layer (see figure S7 (b)), analyzing the deviation in positive and negative direction from the nominal thickness, which differ due to the nonlinearity of the lifetime to distance conversion.

In figure S7 c) we show the estimated sample roughness $\Delta z = [z(\tau+\Delta\tau) - z(\tau-\Delta\tau)]/2$ and compare it with the nominal thickness of each spacer layer – semi-log plot of, blue circles. We find an exponential increase of the estimated roughness over the thickness (previous have reported this behavior [1]) which, for $4 < z < 50$ nm yields a ratio σ/z roughly around 10%, which we take as small enough to guarantee the accurateness of our experimental verification. Moreover, to validate our estimations, we plot the RMS roughness measured by AFM as function of the spacer layer thickness (figure S7 (c), black circles) and obtain a very similar exponential trend line.

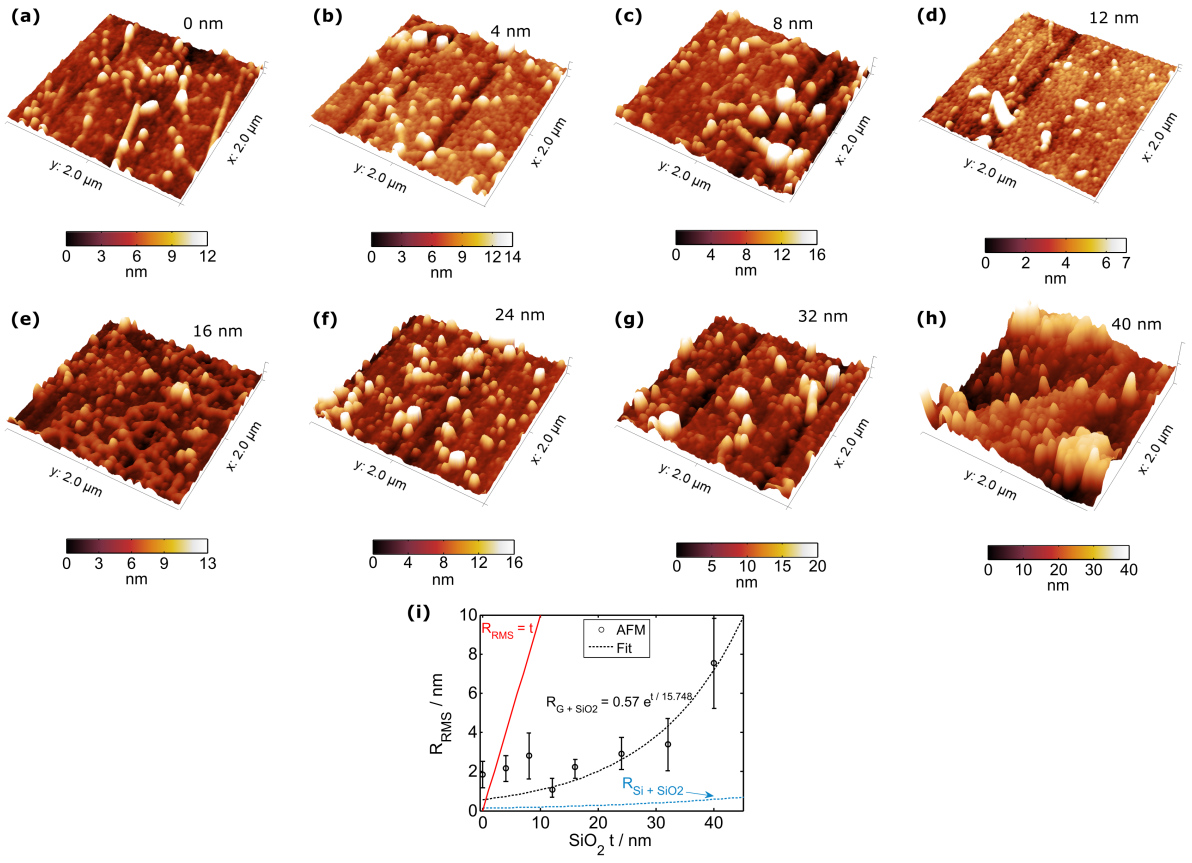

Figure S6. AFM images of experimental verification sample composed of cover glass + graphene + SiO_2 spacer layer + PVA Atto488. (a – h) spacer layers with nominal thickness of 0, 4, 8, 12, 16, 24, 32 and 40, respectively. (i) Plot of RMS roughness as function of spacer thickness and exponential curve fitting and comparing to the nominal thickness (red) and the RMS roughness found for SiO_2 on Si substrate (blue).

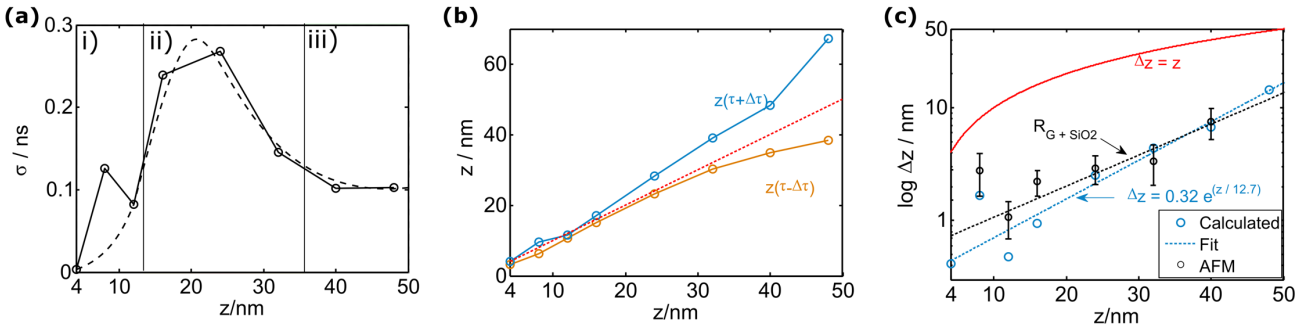

Figure S7: Analysis of the errors potentially caused by surface roughness. a) Width of the FLIM distributions (shown in figure 2(c) in dependence of the nominal spacer, b) Estimation of roughness via the standard deviation in resulting Δz, c) Distance uncertainty via

S6. Additional experiments on the steady state "on"-"off" sensing capability

We repeat the static "on-off" testing of the Atto488@hp-DNA on functionalize graphene genosensing platform on a different graphene sample and perform the same data analysis as described in the main text of this article. The results are displayed in figure S5. A larger variety of fluorescence characteristics are found, besides areas that are quenched and change to an un-quenched state after addition of target DNA, in addition, areas with low intensity that remain of low intensity also after addition of target DNA are observed. Provided that the concentration of Atto488@hp-DNA probes used is high and allows for a full coverage of the graphene areas, we assume the regions remaining of low fluorescence intensities during and after the target DNA binding reaction are free of graphene, and therefore, free of Atto488@hp-DNA probes.

The nanoscale displacement $\Delta z = 9.4 \pm 0.7$ nm is found (see figure S5(k)), which is in nearly perfect agreement with our estimation of 9.5 nm of the molecular length of the DNA strand.

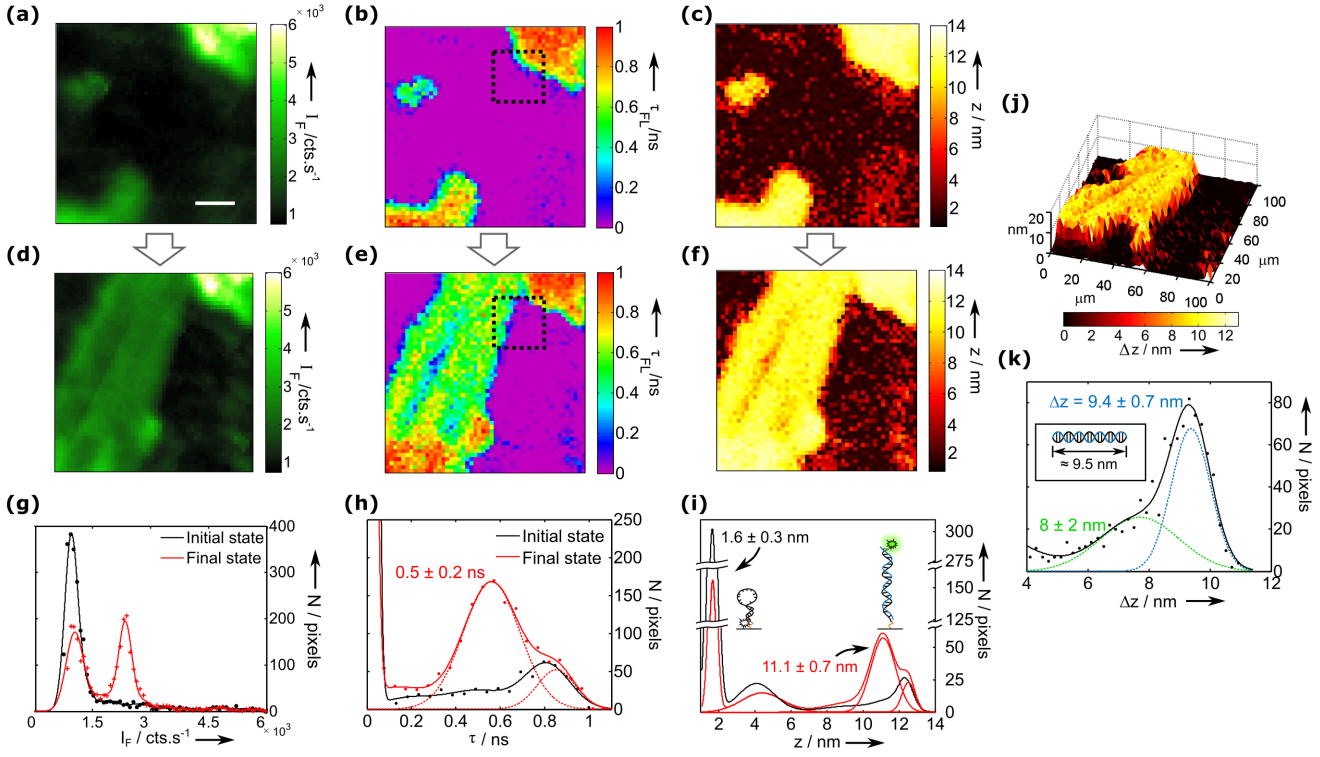

Figure S8. Characterization of a the Atto488@hp-DNA-Graphene sensing platform before and ≈4 h after addition of target DNA. (a-c) Initial state of the reaction characterized by 2D mappings of the fluorescence intensity: I_F (a), fluorescence lifetime: t_{FL} (b) and nanoscale distance from the graphene surface: z (c). The latter is calculated from the fluorescence lifetime image (b) using a theoretical RET model formulated by Gaudreau et al. for graphene. [9] (d-f) Final state of the reaction characterized by the same quantities as and (i) correspondence with (a-c).The distributions and Gaussian curve-fittings characterizing the initial and final states for each quantity are plotted in (g-i). (j) Displacement of the Atto 488 dyes (Δz). (k) Distribution of nanoscale displacement of the dyes at the final state of the DNA hybridization reaction. The scale bar is 20 μm and the same.

S7. Additional experiments of the real-time DNA hybridization

A time-lapse series of FLIM images of the Atto488@hp-DNA graphene functionalized sensing platform was obtained in an area indicated in figure S5 (dotted square). The FLIM images of the time-lapse series, were obtained over a time-span of 105 min, with a time resolution of ≈ 13 min and in figure S6 the Atto488@hp-DNA labeled regions were analyzed and fluorescence lifetimes given in color code.

In figure S7 two additional experiments for real-time DNA hybridization sensing with nanoscale sensitivity are shown as a confirmation of the reproducibility of this method. Again we consider only those parts of the images where the hybridization reaction is observed for the determination of the nanoscale distance distributions over time.

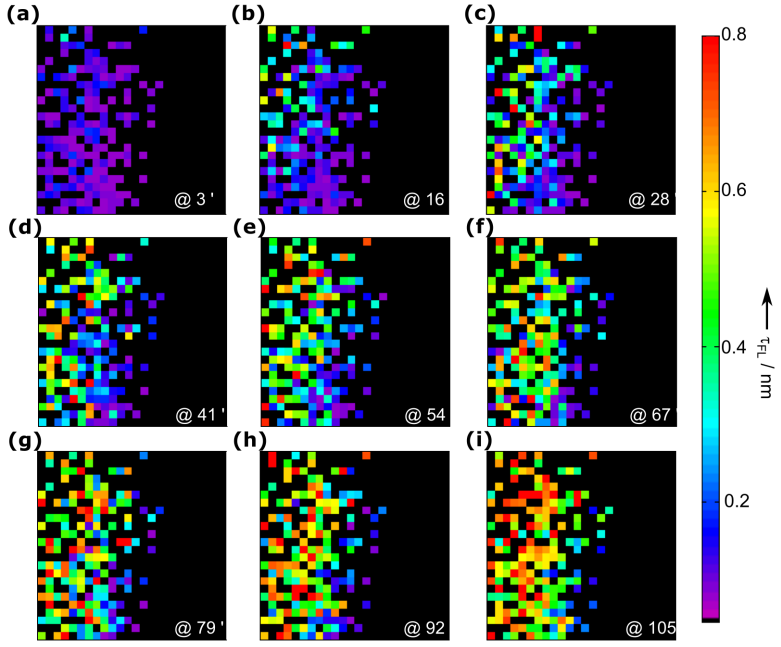

Figure S9. FLIM images from a time-lapse series taken after addition of target DNA solution onto the Atto488@hp-DNA–graphene functionalized sensing platform. Imaging times after the addition of target DNA from (a)-(i) are 3, 16, 28, 41, 54, 67, 79, 92 and 105 minutes, respectively. The scale bar is 5 μm and the same for all images.

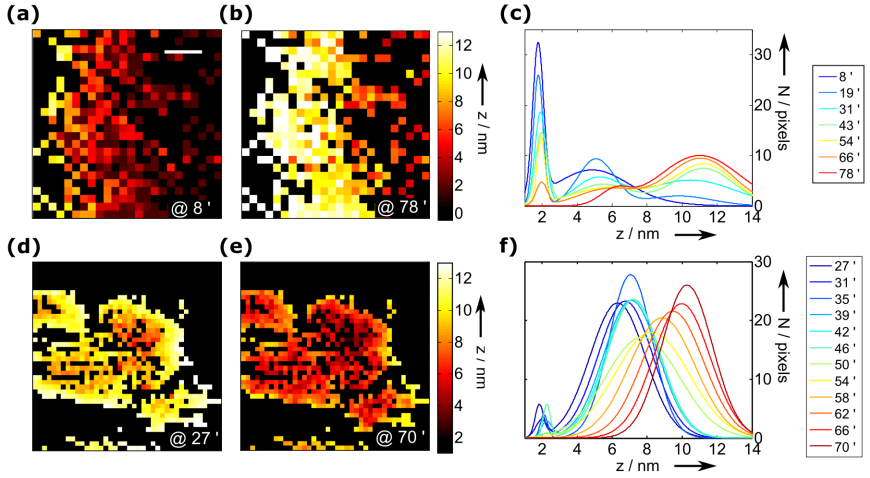

Figure S10. Results from two complementary experiments using time-lapse FLIM to study the DNA hybridization reaction in as-prepared Atto488@hp-DNA graphene functionalized sensing platform samples. (a-b) nanoscale distance (z) of the Atto 488 dyes from the graphene surface at time points 8 and 78 minutes, respectively. Grayed-out points display no signs of occurrence of DNA hybridization and were therefore ignored. (c) Distribution of z in the colored areas of (a) and (b) calculated for the full time-lapse data series. Time points indicated in the legend. (d-f) are analogous to (a-c), for an as-prepared sample. The scale in (a) is 5 μm long and the same for (b). The scale bar in (d) is 4 μm long and the same for (e).

REFERENCES

[1] Connell Group 2009 Selected Bond Energies and Bond Lengths

[2] Kiralj R eta Ferreira M M C 2002 On Heteroaromaticity of Nucleobases. Bond Lengths as Multidimensional Phenomena *J. Chem. Inf. Comput. Sci.* **43** 787–809

[3] Förster T 1948 Zwischenmolekulare Energiewanderung und Fluoreszenz *Ann. Phys.* **437** 55–75

[4] Swathi R S eta Sebastian K L 2009 Long range resonance energy transfer from a dye molecule to graphene has (distance)-4 dependence *J. Chem. Phys.* **130** 86101

[5] Salihoglu O, Kakenov N, Balci O, Balci S eta Kocabas C 2016 Graphene as a Reversible and Spectrally Selective Fluorescence Quencher *Sci. Rep.* **6** 33911

[6] Medintz I eta Hildebrandt N 2013 *FRET - Förster Resonance Energy Transfer* (Weinheim: Wiley-VCH, Weinheim)

[7] Swathi R S eta Sebastian K L 2009 Distance dependence of fluorescence resonance energy transfer *J. Chem. Sci.* **121** 777–87

[8] Swathi R S eta Sebastian K L 2008 Resonance energy transfer from a dye molecule to graphene *J. Chem. Phys.* **129** 1–9

[9] Gaudreau L, Tielrooij K J, Prawiroatmodjo G E D K, Osmond J, García de Abajo F J eta Koppens F H L 2013 Universal Distance-Scaling of Non-radiative Energy Transfer to Graphene *Nano Lett.* **13** 2030–5

[10] Nair R R, Blake P, Grigorenko A N, Novoselov K S, Booth T J, Stauber T, Peres N M R eta Geim A K 2008 Fine Structure Constant Defines Visual Transparency of Graphene *Science (80-.).* **320** 1308

[11] Federspiel F, Froehlicher G, Nasilowski M, Pedetti S, Mahmood A, Doudin B, Park S, Lee J-O, Halley D, Dubertret B, Gilliot P eta Berciaud S 2015 Distance dependence of the energy transfer rate from a single semiconductor nanostructure to graphene *Nano Lett.* **15** 1252–8

[12] Gao L, Lemarchand F eta Lequime M 2012 Exploitation of multiple incidences spectrometric measurements for thin film reverse engineering. *Opt. Express* **20** 15734–51

[13] Greasley S, Jhoti H, Fensome A C, Cockcroft S, Thomas G M H eta Bax B 1994 Crystallization and Preliminary X-ray Diffraction Studies on ADP-ribosylation Factor 1 *J. Mol. Biol.* **244** 651–3

[14] Chroma Technology Corporation 2017 Spectra Viewer – Atto 488 | Chroma Technology Corp

[15] Meshkova A S, Starostin S A, Van De Sanden M C M eta De Vries H W 2018 Variable roughness development in statically deposited SiO2 thin films: A spatially resolved surface morphology analysis *J. Phys. D. Appl. Phys.* **51**